REPORT DOCUMENTATION PAGE

The public reporting burden for this collection of information is estimated to average 1 hour per response, including the time for reviewing instructions, searching existing data sources, gathering and maintaining the data needed, and completing and reviewing the collection of information. Send comments regarding this burden estimate or any other aspect of this collection of information, including suggestions for reducing the burden, to Department of Defense, Washington Headquarters Services, Directorate for Information Operations and Reports (0704-0188), 1215 Jefferson Davis Highway, Suite 1204, Arlington, VA 22202-4302. Respondents should be aware that notwithstanding any other provision of law, no person shall be subject to any penalty for failing to comply with a collection of information if it does not display a currently valid OMB control number.
PLEASE DO NOT RETURN YOUR FORM TO THE ABOVE ADDRESS.

1. REPORT DATE (DD-MM-YYYY)	2. REPORT TYPE Journal Article	3. DATES COVERED (From - To)

4. TITLE AND SUBTITLE
Quantitative Environmental Cell - Transmission Electron Microscopy: Studies of Microbial Cr(VI) and Fe(III) Reduction

5a. CONTRACT NUMBER

5b. GRANT NUMBER

5c. PROGRAM ELEMENT NUMBER
602233N

6. AUTHOR(S)
Tyron Daulton, Brenda J. Little, Jin Kim, Steven Newell, Kristine Lowe, Y. Furukawa, J. Jones-Meehan and Dawn Lavoie

5d. PROJECT NUMBER

5e. TASK NUMBER

5f. WORK UNIT NUMBER

7. PERFORMING ORGANIZATION NAME(S) AND ADDRESS(ES)
Naval Research Laboratory
Oceanography Division
Stennis Space Center, MS 39529-5004

8. PERFORMING ORGANIZATION REPORT NUMBER
NRL/JA/7303/02/0001

9. SPONSORING/MONITORING AGENCY NAME(S) AND ADDRESS(ES)
Office of Naval Research
800 N. Quincy St.
Arlington, VA 22217-5660

10. SPONSOR/MONITOR'S ACRONYM(S)

11. SPONSOR/MONITOR'S REPORT NUMBER(S)

12. DISTRIBUTION/AVAILABILITY STATEMENT
Approved for public release; distribution is unlimited

20040203 121

13. SUPPLEMENTARY NOTES

14. ABSTRACT
Several applications of environmental cell (EC)-transmission electron microscopy (TEM) to microbial metal reduction studies are reviewed. Electron energy loss spectroscopy (EELS) techniques were used to determine oxidation state, at high spatial resolution, of Cr associated with the metal-reducing bacteria, Shewanella oneidensis, in anaerobic cultures containing Cr(VI)C>42-. These techniques were applied to fixed cells examined in thin section by conventional TEM and unfixed, hydrated bacteria examined by EC-TEM. Measurements by EELS demonstrated that cell boundaries became saturated with low concentrations of Cr and the precipitates encrusting bacterial cells contained a reduced form of Cr in oxidation state +3 or lower. In addition, reduction by S. oneidensis of structural Fe(lll) in nontronite, an expandable clay, was studied under anaerobic conditions. Direct observations by EC-TEM yield unambiguous measurement of layer spacings and the contraction of hydrated, clay layers upon reduction of structural Fe(lll). In particular, nonreduced and Fe(l Unreduced nontronite, observed by EC-TEM, exhibit mean (001) spacings of 1.50 nm and 1.26 nm, respectively.

15. SUBJECT TERMS
(EC)-transmission, microbial metal reduction, anaerobic cultures

16. SECURITY CLASSIFICATION OF:			17. LIMITATION OF ABSTRACT	18. NUMBER OF PAGES	19a. NAME OF RESPONSIBLE PERSON Brenda Little
a. REPORT	b. ABSTRACT	c. THIS PAGE			
Unclassified	Unclassified	Unclassified	SAR	15	19b. TELEPHONE NUMBER (Include area code) 228-688-5494

PUBLICATION OR PRESENTATION RELEASE REQUEST

Pubkey: 3173 NRLINST 5600.2

1. REFERENCES AND ENCLOSURES	2. TYPE OF PUBLICATION OR PRESENTATION	3. ADMINISTRATIVE INFORMATION

1. REFERENCES AND ENCLOSURES

Ref: (a) NRL Instruction 5600.2
(b) NRL Instruction 5510.40D

Encl: (1) Two copies of subject paper
(or abstract)

2. TYPE OF PUBLICATION OR PRESENTATION

( ) Abstract only, published ( ) Abstract only, not published
( ) Book ( ) Book chapter
( ) Conference Proceedings ( ) Conference Proceedings
 (refereed) (not refereed)
( ) Invited speaker ( ) Multimedia report
( ) Journal article (refereed) (X) Journal article (not refereed)
( ) Oral Presentation, published ( ) Oral Presentation, not published
( ) Other, explain

3. ADMINISTRATIVE INFORMATION

STRN NRL/JA/7303-02-1
Route Sheet No. 7303/
Job Order No.
Classification ___X___ U ____ C
Sponsor
approval obtained ___X___ yes ____ no

4. AUTHOR

Title of Paper or Presentation

Quantitative Environmental Cell - Transmission Electron Microscopy: Studies of Microbial Cr(VI) and Fe(III) Reduction

Author(s) Name(s) (First,MI,Last), Code, Affiliation if not NRL

Tyrone Daulton, Brenda J. Little, Jin Kim, Steven Newell, Kristine Lowe, Y. Furukawa, J. Jones-Meehan, Dawn Lavoie

It is intended to offer this paper to the _____
                                                                (Name of Conference)

_____
(Date, Place and Classification of Conference)

and/or for publication in   **JEOL News, Unclassified**
                                            (Name and Classification of Publication)   (Name of Publisher)

After presentation or publication, pertinent publication/presentation data will be entered in the publications data base, in accordance with reference (a).

It is the opinion of the author that the subject paper (is ____) (is not __X__) classified, in accordance with reference (b).

This paper does not violate any disclosure of trade secrets or suggestions of outside individuals or concerns which have been communicated to the Laboratory in confidence. This paper (does ____) (does not __X__) contain any militarily critical technology.

This subject paper (has ____) (has never __X__) been incorporated in an official NRL Report.

Brenda J. Little, 7330	_Brenda J. Little_
Name and Code (Principal Author)	(Signature)

5. ROUTING/APPROVAL

CODE	SIGNATURE	DATE	COMMENTS
Author(s) Little	_Brenda J. Little_	02/08/02	
Section Head N/A			
Branch Head N/A			
Division Head William J. Jobst, 7300	_W. Jobst_	2/8	1. Release of this paper is approved. 2. To the best knowledge of this Division, the subject matter of this paper (has ___) (has never __X__) been classified.
Security, Code 7030.1	_David R. _____	2/12	1. Paper or abstract was released. 2. A copy is filed in this office @ SSC-C80
Office of Counsel, Code 1008.3	_Susan Sellers for _____ Beck_	2/13	
ADOR/Director NCST	_Edward R. Franchi_	2/20/0	E.R. FRANCHI, ACTING, ADOR 70
Public Affairs (Unclassified/ Unlimited Only), Code 7030.4	_W. M. Barr_	2/12	
Division, Code			
Author, Code			

HQ-NRL 5511/6 (Rev. 12-98) (e)   THIS FORM CANCELS AND SUPERSEDES ALL PREVIOUS VERSIONS

[X] **A - Approved for public release, distribution is unlimited.**

[ ] **B - Distribution authorized to U.S. Government agencies only** (*check reason below*):

- [ ] Foreign Government Information
- [ ] Proprietary Information
- [ ] Test and Evaluation
- [ ] Contractor Performance Evaluation
- [ ] Administrative/Operational Use
- [ ] Software Documentation
- [ ] Critical Technology
- [ ] Premature Dissemination
- [ ] Cite "Specific Authority _____"

(*Identification of valid documented authority*)

Date statement applied _____

Other requests for this document shall be referred to _____

(*Insert Controlling DOD Office*)

[ ] **C - Distribution authorized to U.S. Government agencies and their contractors** (*check reason below*):

- [ ] Foreign Government Information
- [ ] Administrative/Operational Use
- [ ] Software Documentation
- [ ] Critical Technology
- [ ] Cite "Specific Authority _____"

(*Identification of valid documented authority*)

Date statement applied _____

Other requests for this document shall be referred to _____

(*Insert Controlling DOD Office*)

[ ] **D - Distribution authorized to DOD and DOD contractors only** (*check reason below*):

- [ ] Foreign Government Information
- [ ] Software Documentation
- [ ] Administrative/Operational Use
- [ ] Critical Technology
- [ ] Cite "Specific Authority _____"

(*Identification of valid documented authority*)

Date statement applied _____

Other requests for this document shall be referred to _____

(*Insert Controlling DOD Office*)

[ ] **E - Distribution authorized to DOD components only** (*check reason below*):

- [ ] Proprietary Information
- [ ] Foreign Government Information
- [ ] Administrative/Operational Use
- [ ] Premature Dissemination
- [ ] Software Documentation
- [ ] Contractor Performance Evaluation
- [ ] Critical Technology
- [ ] Direct Military Support
- [ ] Test and Evaluation
- [ ] Cite "Specific Authority _____"

(*Identification of valid documented authority*)

Date statement applied _____

Other requests for this document shall be referred to _____

(*Insert Controlling DOD Office*)

[ ] **F - Further dissemination only as directed by** _____

(*Insert Controlling DOD Office*)

Date statement applied _____ or higher DOD authority _____

[ ] **G - Distribution authorized to U.S. Government agencies and private individuals or enterprises eligible to obtain export-controlled technical data in accordance with regulations implementing 10 U.S.C. 140c.**

Date statement applied _____

Other requests for this document shall be referred to _____

(*Insert Controlling DOD Office*)

*For NRL publications, this is usually the Commanding Officer, Naval Research Laboratory, Washington, DC 20375-5320

7. OTHER LIMITATION

[ ] Classification   [ ] NOFORN   [ ] DTIC exempt (explain) _____

Classification Review
(initial/Date)

Substantive changes made in this document after approval by Classification Review and Public Release invalidate these reviews. Therefore, if any substantive changes are made by the author, Technical Information, or anyone else, the document must be returned for another Classification Review and Publication Release.

8. INSTRUCTIONS

Author completes and submits this form with the manuscript via line channels to the division head for review and approval according to the routing in Section 4.

1. NRL Reports..........Submit the diskette (if available), manuscript, typed double-spaced, complete with tables, illustrations, references, draft SF 298, and proposed distribution list.

2. NRL Memorandum Reports..........Submit a copy of the original, typed manuscript complete with tables, illustrations, references, draft SF 298, and proposed distribution list.

3. NRL Publications or other books, brochures, pamphlets, proceedings, or any other printed publications..........Handled on a per case basis by Site Technical Information Office.

Quantitative Environmental Cell - Transmission Electron Microscopy: Studies of Microbial Cr(VI) and Fe(III) Reduction

Tyrone L. Daulton[†], Brenda J. Little[††], Jin W. Kim[†], Steven Newell[†], Kristine Lowe[†††], Yoko Furukawa[†], Joanne Jones-Meehan[†††] and Dawn L. Lavoie[†]

[†††]**Marine Geosciences Division, Naval Research Laboratory**
[†††]**Oceanography Division, Naval Research laboratory**
[†††]**Chemistry Division, Naval Research Laboratory**

[†]Stennis Space Center, MS, 39529 USA
[†]E-mail :tdaulton@nrlssc.navy.mil

Several applications of environmental cell (EC)-transmission electron microscopy (TEM) to microbial metal reduction studies are reviewed. Electron energy loss spectroscopy (EELS) techniques were used to determine oxidation state, at high spatial resolution, of Cr associated with the metal-reducing bacteria, *Shewanella oneidensis*, in anaerobic cultures containing $Cr(VI)O_4^{2-}$. These techniques were applied to fixed cells examined in thin section by conventional TEM and unfixed, hydrated bacteria examined by EC-TEM. Measurements by EELS demonstrated that cell boundaries became saturated with low concentrations of Cr and the precipitates encrusting bacterial cells contained a reduced form of Cr in oxidation state +3 or lower. In addition, reduction by *S. oneidensis* of structural Fe(III) in nontronite, an expandable clay, was studied under anaerobic conditions. Direct observations by EC-TEM yield unambiguous measurement of layer spacings and the contraction of hydrated, clay layers upon reduction of structural Fe(III). In particular, nonreduced and Fe(III)-reduced nontronite, observed by EC-TEM, exhibit mean (001) spacings of 1.50 nm and 1.26 nm, respectively.

Introduction

Conventional transmission electron microscopy (TEM) studies of microbial reduction of metals have provided important information. However, they are limited because the techniques of fixation, embedding, and microtoming, necessary to prepare thin specimens, are known to alter delicate cellular and abiotic microstructures. Fixation and dehydration preserve some cellular structure, but buffer and organic solvent washes remove extracellular polymers. In addition, soluble ions from extracellular and intracellular sources, such as soluble reduction intermediates, can be lost. Reduction intermediates are unstable with intermediate valence state between the valances of the stable end members of the reduction process. Dehydration causes basal layer spacings in expandable clay minerals to contract and the extracellular biopolymers produced by bacteria associated with clays to collapse into a filamentous, web-like network. In contrast, environmental cell (EC)-TEM is a powerful technique in which hydrated specimens can be examined at high spatial resolution in more or less their natural state. The purpose of this paper is to demonstrate the application of EC-TEM for the study of microbial metal reduction mechanisms and their alteration products; two studies are reviewed.

Microbial reduction of Cr(VI)

Hexavalent chromium species are strong oxidants which act as carcinogens, mutagens, and teratogens in biological systems [1]. The high solubility, bioavailability, and toxicity of Cr(VI) make it a particular environmental concern. Microbial mechanisms for Cr(VI) reduction are of particular technological and biological importance because they convert a toxic, mobile element into a less toxic, immobile form. The study of microbial Cr(VI) reduction, such as the identification of reduction intermediates, has been hindered by the lack of an analytical technique that can determine the oxidation state of Cr at subcellular spatial resolution. The most widely used method for following Cr(VI) reduction is the diphenylcarbazide colorimetric method [2]. Other methods used to determine oxidation state in bacterial cultures include electron spin resonance (ESR) (also called electron paramagnetic resonance (EPR) and electron magnetic resonance (EMR)) spectroscopy, and X-ray photoemission spectroscopy (XPS). These bulk techniques cannot provide detailed information at the subcellular (submicron) level necessary for understanding microbial reduction processes.

Both TEM and scanning electron microscopy (SEM) have sufficient resolution to study the spatial relationship between cells and reduction products, as well as their chemistry. For example, energy-dispersive X-ray spectroscopy (EDXS) has been used to identify elements present in reduction products associated with bacteria [3-8] and wetland plants [9]. However, EDXS is insensitive to oxidation state. Electron energy loss spectroscopy (EELS) by TEM is a direct probe of the electron configuration around atoms, and can determine the oxidation state of $3d$ and $4d$ transition metals at high spatial resolution [10, 11]. Furthermore, EELS techniques have been used to produce oxidation state maps using energy filtered imaging [12].

Determination of oxidation state by EELS is accomplished by analyzing valence induced differences in fine structure of L_2 and L_3 (or collectively $L_{2,3}$) absorption edges by comparison of unknowns to standards of known oxidation state. The $L_{2,3}$ absorption edges arise from transitions to unoccupied d levels from two spin-orbit split levels, $2p_{1/2}$ level (producing the L_2 edge) and the $2p_{3/2}$ level (producing the L_3 edge). The valence of a transition metal is related to the number of holes in the d level (i.e. the $3d^n$ or $4d^n$) configuration. For example, tetrahedral Cr(VI) has an empty d orbital ($3d^0$ configuration) and octahedral Cr (III) has a $3d^3$ configuration. Since $L_{2,3}$ absorption edges are inherently dependent on the number of unoccupied d levels in $3d$ and $4d$ transition metals, they are sensitive to valence state. In general, oxidation state can affect the position, shape and relative intensity of $L_{2,3}$ absorption edges. Techniques used to determine mixed/single valence states involve analysis of the following: (a) the position of the $L_{2,3}$ absorption edges [10], (b) the ratio of the $I(L_3)$ / $I(L_2)$ integrated-peak intensity (henceforth abbreviated L_3/L_2) [10, 11], and (c) least squares fits of summed spectra of standards or calculations to the shape of $L_{2,3}$ absorption edges [13].

Because of difficulties in the application of EELS techniques to actual microcharacterization of mineral oxidation state, these techniques have been under utilized. For example, despite the detailed, submicron-scale information EELS techniques can provide, to our knowledge, they have never been applied in microbial reduction studies. In fact, previous TEM studies assumed

microbial Cr(VI) reduction products were Cr(III) [6, 8]. Since Cr(III) is a stable and insoluble reduced form, this assumption is likely correct. However, the oxidization state of the Cr associated with bacteria has not yet been determined by direct measurement. We recently demonstrated the application of EELS techniques for the determination of oxidation state of metals associated with hydrated bacteria [14]. In particular, Cr(VI) reduction by *Shewanella oneidensis* [15] was studied.

Basal layer contraction of expandable clays induced by Fe(III) reduction

Bacteria have been shown to effectively reduce octahedral Fe(III) in clays [16, 17]. The importance of the role of redox driven interactions between ferruginous clays and bacteria in the alteration of clays has been receiving increasingly more attention. For example, swelling pressures of ferruginous clays are related to basal layer spacing [18], which depends on the oxidation state of octahedral Fe [19]. Furthermore, reduction of Fe(III) in ferruginous clays produces decreased swelling pressures [20], increased cation fixation [21], smaller specific surface area [22], and a decrease in mean layer spacing [23]. Interlayer force is believed produced by the mutual attraction to interlayer cations by the net-negative charge of phyllosilicate layer surfaces which balances the total charge of the clay. Therefore these studies suggest, increased interlayer force may be driven by reduction-induced changes in the surface layer charge. However, this theory cannot be fully evaluated because of the lack of direct measurements. Nearly all structural data have been obtained by bulk techniques, and data available by direct measurements are inconclusive, e.g. [24].

Stuki and Tessier [24] examined chemically reduced Fe-rich smectite by high resolution (HR)-TEM. Specimens were prepared by thin section after water exchange with embedding resin. Using selected area electron diffraction (SAED), they showed the crystal stacking changed from turbostratic to a more ordered structure in the reduced state, indicating an increase of interlayer attraction due to the structural reduction of Fe(III) to Fe(II). However, the expected contraction in clay (001) layer spacing was not found. A constant layer spacing of 1.26 nm was observed in both oxidized and reduced smectite. This measurement is in conflict with the earlier *in-situ* pressure-cell X-ray diffraction work of Wu *et al.* [23] which demonstrated a decrease in mean interlayer distance upon reduction of Fe(III) in bulk Na-nontronite. However, the effects of resin infiltration on the interlayer spacing are uncertain and, therefore, the homogeneous layer spacing observed by Stuki and Tessier [24] may be due to artifacts induced by resin infiltration. We recently demonstrated the application of EC-TEM to study the collapse of basal spacing in ferruginous-expandable clays induced by microbial Fe(III) reduction [25]. The effects of anaerobic respiration (Fe(III) reduction) by *S. oneidensis* on nontronite were examined. In particular, differences in layer spacings between nonreduced and reduced nontronite, in their 'native' hydrated state, were characterized using EC-TEM.

Cultures, Methods, and Techniques

Cultures

S. oneidensis [15] was originally isolated from the anaerobic zone of Mn-rich sediments in Oneida Lake, NY [26]. *S. oneidensis* (ATCC RF50108) is a Gram-negative bacterium capable of respiring aerobically and anaerobically using a variety of terminal electron acceptors, including: O_2, Fe(III), Mn(IV), nitrite (NO_2-), nitrate (NO_3-), sulfite (SO_3^{2-}), thiosulfate ($S_2O_3^{2-}$), tetrathionate ($S_4O_6^{2-}$), trimethylamine N-oxide, fumarate, glycine, Cr(VI), U(VI), and Tc(VII) [27-29]. Complete details on the cultures and reduction experiments can be found in [14, 25], and are summarized below.

For conventional-TEM studies of Cr(VI) reduction, cells were grown anaerobically for 30 days with 100 μM CrO_4^{2-} as the sole terminal electron acceptor. Samples (1 mL) were pelleted by centrifugation, fixed in 1 mL of a 5% aqueous solution of glutaraldehyde overnight at room temperature, and embedded in Spurr's resin. The embedded specimen was sectioned to 80 nm thickness by microtome, and mounted on amorphous carbon (a-C) coated Cu TEM grids (see [14] for full description).

For EC-TEM studies of Cr(VI) reduction, cells were grown anaerobically with 100 μM CrO_4^{2-} as the sole terminal electron acceptor. A total of 0.275 moles K_2CrO_4 was added to the culture over a 51-day incubation. In contrast to conventionally prepared TEM specimens, EC-TEM specimen preparation was minimal: culture was centrifuged, supernatant removed, and the pellet rinsed with distilled water to remove trace salts. An aliquot (several μL) of the resuspended pellet was quickly loaded into the EC-specimen holder. Removal of trace salts from the culture circumvented salt precipitation on the EC window as the bulk of the aliquot evaporated, leaving a thin hydrated layer. The specimen was examined at 100 Torr of air (saturated with water vapor) circulating through the EC at a rate of $\approx$ 2 Torr L min^{-1}.

For studies of clay reduction, nontronite from Uley graphite mine, South Australia (Clay Mineral Society standard (NAu-1) [30]) was used as the sole terminal electron acceptor. Samples (diameters < 2.0 μm) were sterilized by exposure to microwave radiation (5 min), and sterility was confirmed from lack of bacterial growth on Luria-Bertani (LB) agar after 2 days. Cells were grown anaerobically with nontronite for 4 days, then examined by EC-TEM at 10 - 100 Torr of air (saturated with water vapor) circulating through the EC at a rate of $\approx$ 2 Torr L min^{-1}.

Transmission electron microscopy

A JEOL JEM-3010 transmission electron microscope operating at 300 keV with a LaB$_6$ filament was used in these studies. This instrument is equipped with an EDXS system, a Gatan imaging filter (GIF200) capable of EELS, and a JEOL EC system. The EC-TEM system is of the closed cell type [31] where confinement of a pressurized environment is achieved with electron-transparent windows. The microscope is equipped with two interchangeable JEOL EC specimen holders (a two-line gas EC and a four-line gas/liquid EC) that are connected to the EC system by flexible, stainless steel lines. Both *in-situ* EC-TEM specimen holders are capable of circulating dry or water-saturated gas (using two lines) at flow rates of 0 - 15 Torr L min^{-1} through the specimen chamber at 10^{-3} to > 200 Torr pressure. The four-line holder has two additional service lines which can be used to independently inject several microliters of liquids from different reservoirs. Each EC holder consists of a
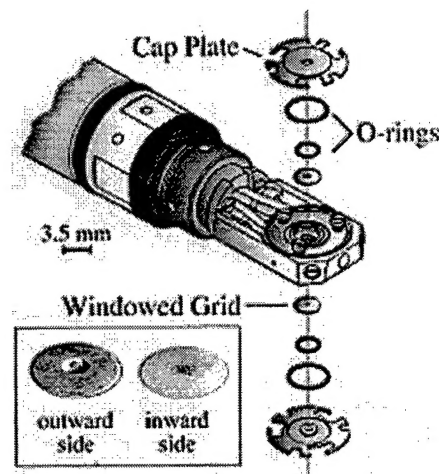
small cylindrical cell sealed by two electron transparent windows on the top and bottom (see **Fig. 1** for the 4-line cell used in this study). The windows are 15 - 20 nm thick amorphous carbon (a-C) films covering seven hexagonally arrayed, 0.15 mm apertures on a 3.5 mm diameter Cu disk (Fig. 1). Prior to use, the windowed grids were tested to withstand a pressure differential of 250 Torr for one minute. A computer controls the EC system and facilitates the operation of inserting, and removing the EC holders from the microscope column without breaching the delicate windows (**Fig. 2**). Higher sensitivity leak checks of the EC windows are performed automatically during the specimen insertion sequence prior to full insertion into the column. Specimens are supported on the lower a-C film window. In conventional TEM, many specimens are supported on a-C films, in this sense, there is only one additional a-C film the electron beam must past through using EC-TEM. Resolution tests of graphite in the EC show lattice resolution of at least 0.38 nm at 60 Torr of hydrated room air. It should be noted that the EDXS system cannot be used with EC-TEM because there is no direct line of sight between the specimen and the EDXS detector.

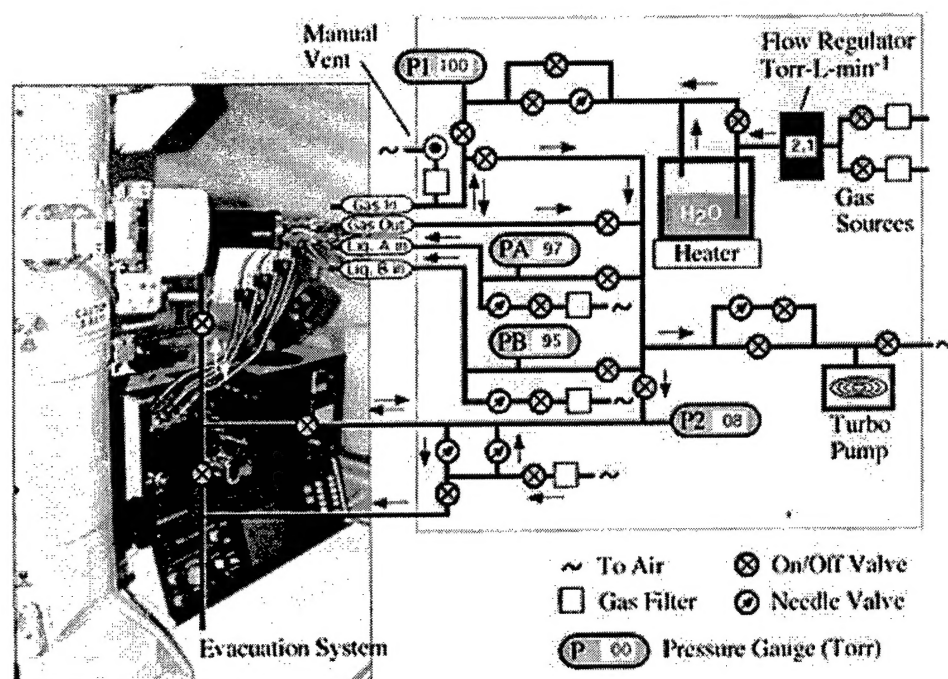Fig. 1. Schematic illustration of the specimen chamber for the four-line EC specimen holder.

Fig. 2. Schematic illustration of the EC control system.

Unlike EC systems based on the principle of differential pumping, closed-cell EC systems require absolutely no modification to the column and the transmission electron microscope can still be used for conventional TEM without compromising resolution and analytical capabilities. The microscope was also equipped with conventional single- and double-tilt specimen holders for conventional TEM. The single-tilt holder has an adapter which accepts windowed EC grids for analysis following their use in the EC holder.

EELS techniques for oxidation state determination

Two EELS techniques were used to identify oxidation state of Cr associated with bacteria. Oxidation state was determined by both the chemical shift of $L_{2,3}$ edges and the ratio of L_3/L_2, integrated-peak intensities, the two most sensitive and straightforward techniques. Results of both techniques are used in

combination to yield higher confidence and accuracy. In contrast, previous EELS studies have focused on demonstrating the capability of one technique, rather than applying techniques in combination to actual microcharacterization in physical/biological systems.

EELS experimental parameters

The following conditions were used during collection of EELS spectra under EC-TEM and TEM conditions: an illumination angle $2\alpha = 4 - 10$ mrad, a collection angle of $2\beta = 10.8$ mrad, a 2 mm entrance aperture, and an energy dispersion of 0.1 eV / channel. Low-loss spectra were acquired with an integration time of 0.128 s and core-loss spectra between 0.512 and 1.02 s. For each acquisition, 10 (EC-TEM) or 25 (conventional TEM) spectra were summed. Spectra were collected in diffraction mode of the transmission electron microscope (i.e. image coupling to the EELS spectrometer) and were corrected for dark current and channel-to-channel gain variation of the charge coupled device (CCD) detector.

Energy calibration of the core-loss regime and measurement of energy drift during data acquisition were performed by collecting zero-loss spectra before and following collection of core-loss spectra. Energy of core-loss spectra was calibrated using the average position of the two zero-loss peaks. The error in the energy calibration corresponded to the energy drift of the zero-loss peaks. In addition, a C-K edge spectrum was acquired immediately following spectrum collection from the O-K / Cr-L core-loss regime. The measured position of the C-K (1s) peak at 284.9 eV (arising from transitions to the π^* molecular orbital) from the TEM a-C support film was used to evaluate the energy calibration. Either the pre-O-K edge background or the pre-Cr-L edge background (depending on the analysis to be performed) was subtracted from core-loss spectra using a power law and plural inelastic scattering was removed by Fourier deconvolution methods [32].

Chromium standards were analyzed by conventional TEM. Standards were produced by placing high purity $Cr(II)F_2$, $Cr(II)Se$, $Cr(III)Cl_3$, $Cr(III)_2O_3$, $KCr(III)(SO_4)_2 \cdot 12H_2O$, and $K_2Cr(VI)O_4$ powders directly on Cu TEM grids coated with holey a-C. Once the standard was prepared, it was examined immediately. For each standard, 20 individual grains were analyzed by EELS. Results were averaged and reported with the statistical standard error.

Results

Direct imaging of Cr(VI) cultures

Examination of *S. oneidensis* in Cr(VI) cultures by EC-TEM, showed the rod-shaped morphology typical of the species (**Fig. 3**). The micrographs demonstrate that bacterial membranes were intact and did not show evidence of rupture from partial decompression. Cells remained hydrated and intact while extracellular polymers surrounding the cells retained moisture. In comparison, unfixed cells deposited on a holy a-C film and examined under high vacuum by conventional TEM (not shown), exhibited ruptured cell membranes, as well as loss of both cell and extracellular polymer mass through dehydration.

Direct imaging revealed two distinct populations of *S. oneidensis* in the

cultures: bacteria exhibiting low image contrast (**Fig. 3a**) and bacteria exhibiting electron dense, high-contrast cell boundaries often encrusted with high-contrast precipitates (**Fig. 3b**). Cross sectional images of bacteria by conventional TEM showed no evidence of intracellular precipitates, suggesting precipitates are restricted to the outer surface of the bacteria. Precipitates ranged in size between ≈10 - 200 nm, and SAED indicated that the grains were predominantly amorphous perhaps due to a high degree of hydration. Often the cells exhibited a 30 - 49 nm thick, high contrast perimeter, indicating that the cell boundary became saturated with elements of heavy mass.

Chemical analysis by EELS of Cr(VI) cultures

Figure 4 shows EELS low-loss and core-loss spectra collected from an encrusted bacterium examined by EC-TEM. The dominant feature in the low-loss spectrum is the zero-loss peak corresponding to electrons which escaped inelastic collisions. The width of the zero-loss peak is a measure of the energy distribution of the incident beam and corresponds to the best energy resolution of the spectrometer (energy resolution typically decreases with increasing energy loss). The narrow zero-loss peak (Fig. 4) shows energy resolution is not significantly affected by transmission through the hydrated, pressurized environment of the EC. The broad feature around 25 eV in the low-loss spectrum corresponds to plasmon excitations (i.e., collective excitations of valence electrons). The ratio of the integrated intensity under the zero-loss and plasmon peaks is related to specimen thickness. The relative height of the two peaks illustrates that multiple scattering is not severe in the EC. The total thickness traversed by the electron beam, estimated by the log-ratio technique [32], is 1.13 λ, where λ is the total mean free path for inelastic scattering through the EC windows and specimen. The low-loss spectrum also exhibits a sharp feature at 13.2 eV that is only observed in EELS spectra collected in the EC. It is consistent with the EELS K-edge of hydrogen [33] which can be produced by electron beam radiolysis of water in the hydrated specimen. For example, similar EELS edges at 13 eV have also been observed concurrently with electron-beam-induced bubble formation from frozen-hydrated biological specimens and were attributed to hydrogen formation [34].

In the core-loss spectrum of encrusted *S. oneidensis* examined by EC-TEM, a strong O-K (1s) edge signal was observed at 537.1 ± 0.5 eV due to H_2O in the hydrated bacterium and extracellular substances. A less intense feature at 529.2 ± 0.5 eV can be attributed to oxygen 2p hybridization with the Cr 3d band, while the broad feature at 558 eV can be attributed to plural (O-K core-loss plus plasmon) scattering. The characteristic pair of Cr-L$_2$ and Cr-L$_3$ edges in the EELS spectrum indicates that the precipitates are Cr-rich.

Bacterial cultures were also examined in cross-section by conventional TEM. Spectra collected from individual precipitates encrusting the outer cell boundary of *S. oneidensis* (**Fig. 5**) showed characteristic Cr-L$_{2,3}$ edges. The sectioned precipitates selected for analysis were those loosely attached to the bacterial outer surface where spectra could be collected without contributions from the bacterial cell. In addition, the electron-dense cell boundary of *S. oneidensis* cells that lacked precipitates encrusting the surface was examined by EELS in cross section. Spectra from the cell boundary revealed characteristic Cr-L$_{2,3}$ edges indicating the cell boundary was saturated with Cr at concentrations likely too low to be detected by EDXS.
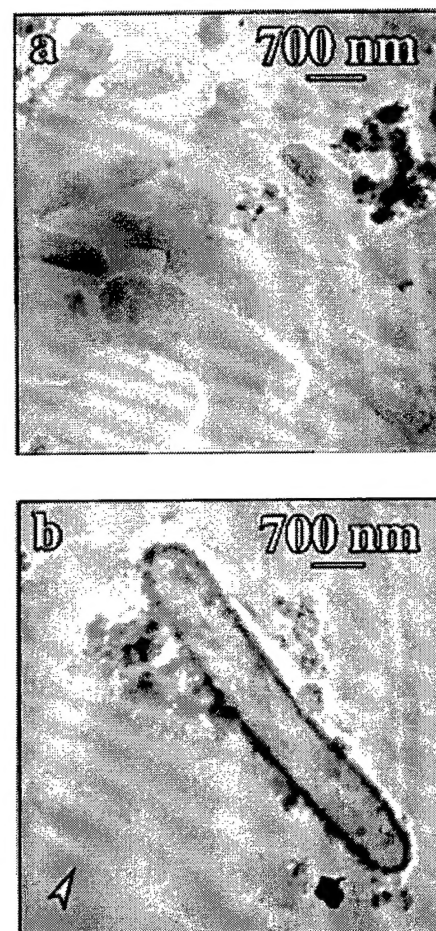
Fig. 3. *Shewanella oneidensis* imaged by EC-TEM at 100 Torr: (a) bacteria exhibiting low contrast in bright-field imaging and (b) bacteria encrusted with electron dense particulate. The arrowhead in panel (b) points to a low contrast bacterium in the same field of view as a bacterium with electron dense particulate, illustrating the dramatic contrast difference.

A comparison of core-loss spectra from encrusted, hydrated *S. oneidensis* (collected by EC-TEM) and Cr standards of known oxidation state (collected by conventional TEM) is shown in **Fig. 6**. The spectrum of $KCr(SO_4)_2 \cdot 12H_2O$ exhibited a peak at 535.7 eV similar to the stronger feature observed in the spectrum from hydrated *S. oneidensis*, and likely corresponds to H_2O bound in the structure. More importantly, systematic differences in Cr-$L_{2,3}$ fine structure are apparent in the spectra of standards (Fig. 6). For example, the Cr-$L_{2,3}$ lines for the standards show a systematic shift in edge-peak energy and variation in relative intensity with oxidation state (Fig. 6). In addition, the Cr-$L_{2,3}$ lines of the K_2CrO_4 peaks are further differentiated in that they appear asymmetric because each is split into two separate peaks separated by ~ 2 eV.

EELS oxidation state analysis of standards

Oxidation state was identified by both the L_3 peak positions and the ratio of L_3/L_2 integrated-peak intensities. Measurement of the L_3 peak positions is straightforward and the results for Cr standards are summarized in **Table 1**. For measurement of the ratio of L_3/L_2 integrated-peak intensities, two methods of background subtraction were used. The first method, illustrated in **Fig. 7**, is similar to the double step function used by [35]. In this method, the Cr-L_3 pre-absorption edge was fit to a power law and subtracted. A linear function was then fit to the Cr-L_2 post-edge region over a 20 eV window (extending from 600 to 620 eV). A linear step function was inserted at the L_2 maximum and a straight line (of the same slope as that fitted to the Cr-L_2 post-edge region) was extrapolated into the L_3 threshold. A second step function was inserted at the L_3 maximum and set to zero below the L_3 maximum. The ratio for the step heights was set at 2:1, consistent with the multiplicity of the initial states, that of four $2p_{3/2}$ electrons and two $2p_{1/2}$ electrons. It should be noted that the ratios of L_3 to L_2 intensities do not follow the expected 2:1 ratio for early $3d$ transition metals [36]. These anomalous ratios can be partially explained by atomic multiplet effects producing overlapping transitions from $2p_{3/2}$ and $2p_{1/2}$ states [37]. Nonetheless, an approximation of 2:1 is sufficient for this work.
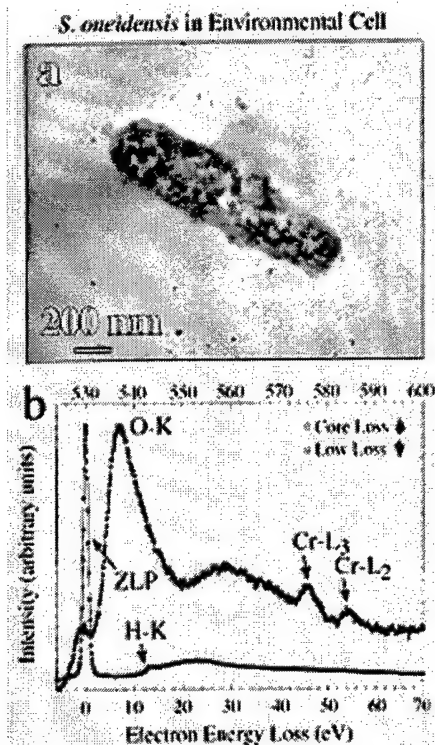

Fig. 4. *Shewanella oneidensis* imaged by EC-TEM at 100 Torr: (a) cell is encrusted with electron dense particulate. (b) EC-TEM EELS spectrum from the bacterium demonstrates the presence of Cr. Both the low-loss spectrum containing the zero-loss peak (ZLP) and the core-loss spectrum of the O-K and Cr-L absorption edges are shown. The full width at half maximum of the ZLP is a measure of the instrumental resolution, which under these EC-TEM conditions is ≈1 eV. As indicated by vertical arrows, the top abscissa corresponds to the low-loss spectrum and the bottom abscissa corresponds to the core-loss spectrum.

Table 1
Cr-L3 (*2p3/2*) and Cr-L2 (*2p1/2*) Adsorption-Edges

XPS-binding energies, EELS L edge peak positions					
Compound	Formal Valence	Cr-L3 (2p3/2) (eV)	Cr-L2 (2p1/2) (eV)	Technique	Reference
Cr	0	573.8 574.0 574.1 574.3 576.5 ± 1.0	583.0 583.4 582.8 585.0 ± 1.0	XPS XPS XPS EELS EELS	[40] [41]a [42]b [43]c [38]d
CrP	0	574.2		XPS	[42]
Cr(CO)6	0	577.6	586.3	XPS	[40]
CrF2	II	574.2 ± 0.1	583.5 ± 0.1	EELS	This study
CrSe	II	574.2 ± 0.1	583.1 ± 0.1	EELS	This study
CrCl3	III	574.9 ± 0.1 576.4	583.4 ± 0.1 587.4	EELS XPS	This study [40]
CrPO4·4H2O	III	576.4 ± 0.2		XPS	[44]b
CuCrO2	III	576.4 ± 0.2	586.2 ± 0.2	XPS	[40] [45]e

$Cr_3(OH)_2(OOCCH_3)_7$	III	576.5 ± 0.2		XPS	[44]b
$NaCrO_2$	III	577.0 ± 0.2	586.9 ± 0.2	XPS	[40] [45]e
Cr_2O_3	III	575.9 ± 0.1 576.4 576.6 - 576.8 576.8 ± 0.2 576.8 576.8 577.9 ± 1.0	584.3 ± 0.1 585.9 586.2 ± 0.2 584.8 586.7 585.8 ± 1.0	EELS XPS XPS XPS EELS XPS EELS	This study [41]a [42] [40] [45]e [46] [47] [38]d
$FeCr_2O_4$	III	576.0	584.0	XPS	[48]f
$KCr(SO_4)_2·12H_2O$	III	576.0 ± 0.1 581.0	584.5 ± 0.1 590.5	EELS XPS	This study [40] [45]e
$LaCrO_3$	III	576.1 ± 0.09	585.8 ± 0.05	XPS	[49]
$LiCrO_2$	III	577.0 ± 0.2	586.8 ± 0.2	XPS	[40] [45]e
$CrOOH$	III	577.0	586.9	XPS	[47]
$Cr(OH)_3·0.4H_2O$	III	576.9 577.1	586.3	XPS XPS	[41]a [42]
CrP	III	577.4		XPS	[42]
$CrCl_3·6H_2O$	III	577.5		XPS	[42]
$CrPO_4$	III	577.8		XPS	[42]
$CrBO_3$	III	578.0		XPS	[42]
$Cr_2(SO_4)·15H_2O$	III	578.6		XPS	[42]
CrO_2	IV	576.3	586.0	XPS	[47]
$LaCrO_4$	V	578.8 ± 0.21	588.0 ± 0.22	XPS	[49]
CrO_3	VI	578.3 ± 0.2 579.0	587.0 ± 0.02 588.2	XPS XPS	[45]e [41]a
$CaCrO_4$	VI	578.9 ± 0.2	588.1 ± 0.2	XPS	[40] [45]e
$BaCrO_4$	VI	579.1 ± 0.2	588.4 ± 0.2	XPS	[40] [45]e
$K_2Cr_2O_7$	VI	579.4 ± 0.2 579.8	588.8 ± 0.2 589.1	XPS XPS	[40] [45]e [47]
$Na_2Cr_2O_7$	VI	579.4 ± 0.2	588.5 ± 0.2	XPS	[40] [45]e
$Rb_2Cr_2O_7$	VI	579.4 ± 0.2	588.7 ± 0.2	XPS	[40] [45]e
$Cs_2Cr_2O_7$	VI	579.5 ± 0.2	588.7 ± 0.2	XPS	[40] [45]e
$SrCrO_4$	VI	579.6 ± 0.2	588.6 ± 0.2	XPS	[40] [45]e
K_2CrO_4	VI	578.6 ± 0.1 579.6 ± 0.2	587.2 ± 0.1 588.9 ± 0.2	EELS XPS	This study [40] [45]e
$PbCrO_4$	VI	578.6 580.9	587.2 587.8 - 589.5	XPS EELS	[48]f [50]
Cs_2CrO_4	VI	579.8 ± 0.2	588.8 ± 0.2	XPS	[40] [45]e
Li_2CrO_4	VI	579.8 ± 0.2	589.0 ± 0.2	XPS	[40] [45]e
Na_2CrO_4	VI	579.8 ± 0.2	589.1 ± 0.2	XPS	[40] [45]e

Fig. 5. *Shewanella oneidensis* imaged by conventional TEM in ≈ 80 nm thick, thin section: (a) cell is encrusted with electron dense particulate. The field of view displays several bacterial cells in random, oblique cross-section. Cross-sectional images show precipitates occur on the outer cell surface and no evidence of intracellular precipitates is observed. (b) EELS spectra from the isolated precipitates demonstrates the presence of Cr. The analyzed precipitates are labeled and the diameter of the circle corresponds to the electron probe diameter.

XPS studies used the Au $4f_{7/2}$ line at 84.0 eV for energy calibration unless otherwise stated.
a) After recalibrating the XPS Au $4f_{7/2}$ line to 84.0 eV from 84.07 eV.
b) Reported as calibrated to XPS Au $4f_{7/2}$ line at 84.0 eV and C (1s) at 284.8 eV.
c) As reported in reference as binding energies.
d) EELS L-edge onsets reported in reference, however L-peak positions are shown here.
e) After recalibrating the XPS Au $4f_{7/2}$ line to 84.0 eV from 82.8 eV.
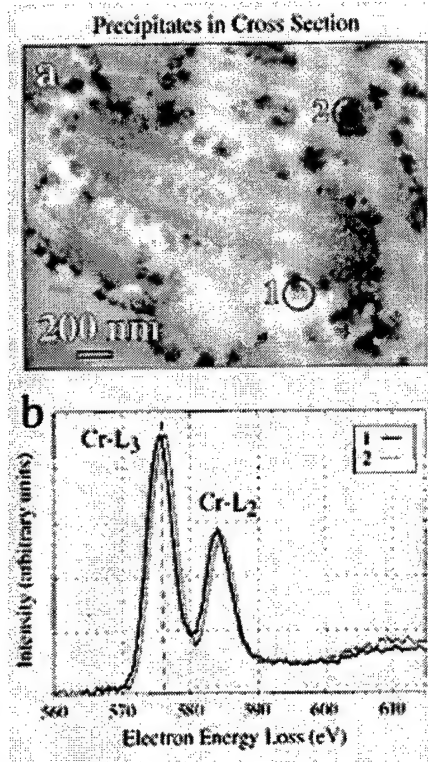f) Energy calibration not reported.

Although the first subtraction method approximates the decreasing background, the fit of $Cr-L_2$ post-edge region was often affected by a broad post-edge feature, containing plural scattering effects not completely removed from the spectra. The post-edge feature varied with each spectrum, introducing scatter in the L_3/L_2 peak ratios. To provide a more consistent background subtraction for all spectra, a second method using a flat, two-step function was applied. The second background fitting procedure is identical to the first except the slope of the linear function is set to zero and it is fit to a 2 eV wide window immediately following the $Cr-L_2$ peak, in the edge tail, prior to the post-edge feature.
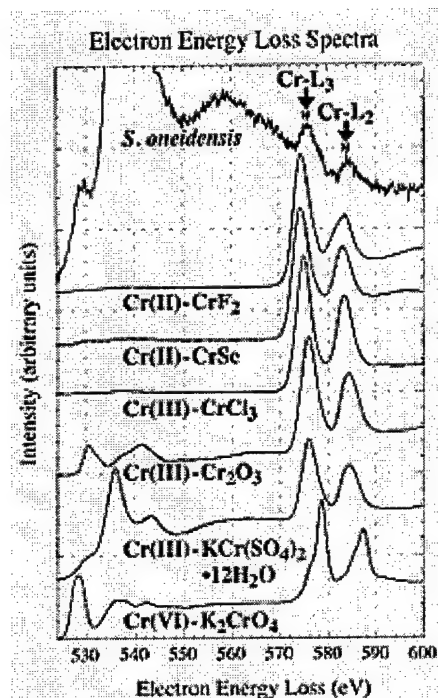
Once the background was subtracted using either of the two methods, the Cr-L peaks were integrated over a 5 eV window. The L_3/L_2 peak ratios for the Cr standards are summarized in **Table 2**. The flat, two-step background subtraction method yielded the lower values, however, less relative scatter in the data. The core-loss spectra for K_2CrO_4 exhibited almost no post L_2 edge features and this may account for the close similarity in L_3/L_2 peak ratios determined using the two background subtraction methods (Table 2). The correlation between measured L_3/L_2 integrated-peak intensity ratios and L_3 peak positions for the Cr oxidation-state standards is shown in **Fig. 8a**. Measurements of the standards demonstrate that Cr oxidation states fall within well-separated regions in the correlation plot. Since the local electronic structure of the atom is responsible for the fine structure of absorption edges, other factors in addition to valence state influence $L_{2,3}$ fine structure. These factors include atom coordination, spin-orbit interactions, crystal field splitting, atomic coulomb repulsion, and exchange effects. For example, within a given oxidation state in Fig. 8a, spectra for the individual standards fall within separate groupings reflecting possible differences from these factors which must be considered to correctly interpret fine structure of absorption edges. The correlation plot represents a map of the possible range in fine structure (including influences from factors other than valence) that a particular Cr oxidation state can display.
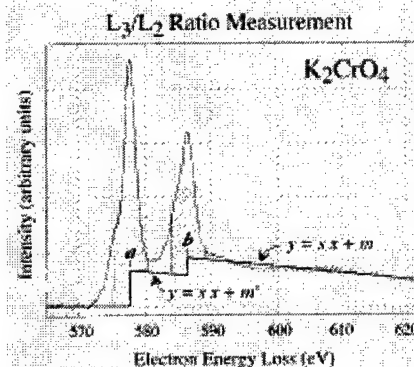

Electron Energy Loss Spectra

Fig. 6. A comparison of the core-loss EELS spectra of encrusted *Shewanella oneidensis* in the EC at 100 Torr and Cr standards of known oxidation state. Spectra were normalized to the intensity of the L_3 peak and offset from one another. The spectra shown for the Cr standards represent the sum of twenty individual spectra. The error bars shown for *S. oneidensis* represent the error in energy loss calibration for that spectrum only. For the errors associated with other spectra, see Table 1.


Table 2 Cr-L Adsorption Edge Ratios			
Compound	Formal Valence	L_3/L_2 Integrated Ratio	
		Background Method I Pearson *et al.* (1993)	Background Method II Flat Two Step
CrF₂	II	2.97 ± 0.07	2.37 ± 0.03
CrSe	II	2.60 ± 0.06	2.04 ± 0.02
CrCl₃	III	1.75 ± 0.03	1.68 ± 0.01
Cr₂O₃	III	1.81 ± 0.01	1.70 ± 0.01
KCr(SO₄)₂·12H₂O	III	1.77 ± 0.02	1.60 ± 0.01
K₂CrO₄	VI	1.42 ± 0.01	1.44 ± 0.01

EELS oxidation state analysis of Cr(VI) cultures

The EELS measurements of the bacterium examined by EC-TEM and precipitates examined in thin section by conventional TEM are summarized in

Table 3. The error reported for the precipitates represents the standard error of the mean of 10 measurements. The errors reported for the encrusted bacteria represent the drift in energy calibration of the spectrometer (L_3 position) and an estimate based on counting statistics (L_3/L_2 ratio).

| Table 3 Cr-L_3(*2p*$_{3/2}$), Cr-L_2(*2p*$_{1/2}$) Adsorption-Edges and L_3/L_2 Integrated Ratios				
Specimen	Cr-L_3 ($2p_{3/2}$)	Cr-$L/2$ ($2p_{1/2}$)	L_3/L_2 Integrated Ratio	
	(eV)	(eV)	Background Method I	Background Method II
Encrusted S. oneidensis	575.7 ± 0.5	584.5 v 0.5	2.75 ± 0.30	1.90 ± 0.30
Isolated precipitates	575.7 ± 0.1	584.3 ± 0.1	1.72 ± 0.02	1.85 ± 0.02
	576.3 ± 0.1	584.7 ± 0.1	1.77 ± 0.02	1.91 ± 0.02

Direct imaging of nontronite cultures

Clay-layer structures in their hydrated state are beam sensitive. Therefore, standard procedures for imaging beam sensitive specimens were employed. Representative examples of high resolution lattice images of nontronite basal layers taken by EC-TEM are shown in **Fig. 9**. The EC-TEM measured distributions of (001) layer spacings in nonreduced and microbially reduced nontronite are shown in **Fig. 10**. Each data point in the distribution represents the mean (001) spacing of a packet of fringes within individual clay grains. Nonreduced nontronite has mean (001) spacing of 1.50 ± 0.08 nm and the microbially Fe(III) reduced form has mean (001) spacing of 1.26 ± 0.10 nm (the errors represent the standard deviation of the population). It is clear from Fig. 10 that the distributions differ and a standard statistical T-test for unpaired data with unequal variance confirms the difference in means is significant. Reduction of Fe(III) in nontronite over 4 days by *S. oneidensis* produced a 0.24 nm contraction in mean (001) layer spacing.
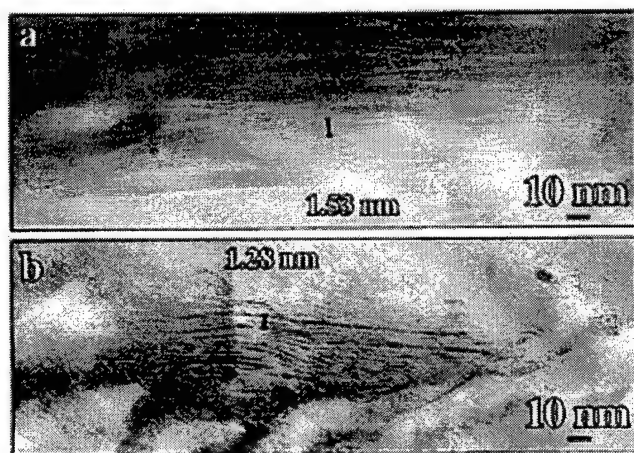
Fig. 9. High resolution lattice images of basal layers of nontronite imaged by EC-TEM at 10 - 100 Torr: (a) nonreduced control and (b) microbial Fe(III) reduced form. The bar illustrates five consecutive basal layer fringes and their average (00l) spacing

Fig. 7. Core-loss EELS spectrum for K_2CrO_4 illustrating the background subtraction used in method I. The step function (bold line) used to subtract the background from the $L_{2,3}$ edges and the areas integrated to yield peak intensities (shaded regions) are shown. The fitting parameters *a, b, s,* and *m* are: the L_3 maximum, the L_2 maximum, the slope of the linear function fitted to the 20 eV post L_2 edge region (600 - 620 eV), and the intercept of the linear function. The parameter *m'* is given by $m' = (2 m - as)/3$.
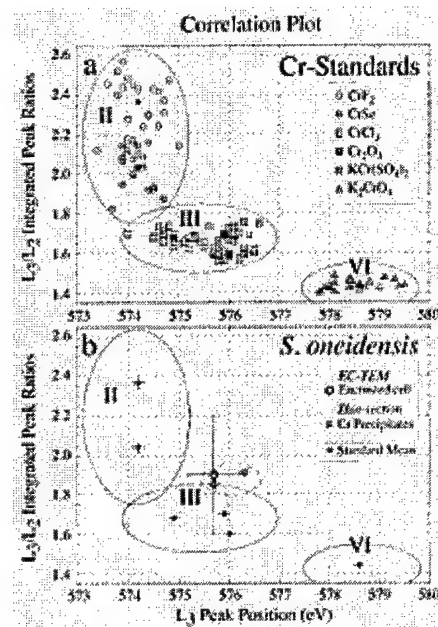
Fig. 8. The correlation between measured L_3/L_2 integrated-peak intensity ratios and L_3 peak positions for a) the Cr oxidation-state standards, b) bacteria and precipitates. Plotted L_3/L_2 ratios were determined using background subtraction method II.

is indicated. There is a range of (001) layer fringe spacings in any one nontronite image. However, the mean spacing is generally smaller for Fe(III)-reduced nontronite than the nonreduced nontronite control (see Fig. 10). The layer fringes annotated by the bars were chosen to contrast the difference in (001) spacings for fringes near the means of the distributions shown in Fig. 10.

Discussion

Oxidation state determination

It is difficult to explicitly deconvolve the influences of atom coordination, spin-orbit interactions, and crystal field splitting on fine structure from those of valence state. Nonetheless, the mean oxidation state of an unknown can be determined by plotting its L_3 peak position and L_3/L_2 integrated-peak intensity ratio in a correlation plot of oxidation state standards (see Fig. 8a). However, it is important that the correlation plot contain the broadest collection of standards feasible to map the full range in fine structure that a particular oxidation state can display. The better these ranges are known, the more confidence can be placed in the oxidation state determination. In this regard, the data in Table 1 supplement that of Fig. 8a. Table 1 includes published $L_{2,3}$ peak positions (absorption edge maximums) from previous EELS studies as well as core-level (or inner-shell) binding energies measured from XPS studies. In XPS, a bulk specimen is illuminated with monochromatic X-rays and the kinetic energies of ejected photoelectrons are measured. The EELS edge onset, the sudden rise in intensity preceding each of the $L_{2,3}$ peaks, represents the ionization threshold which approximately corresponds to the inner-shell binding energy measured by XPS. The difference in chemical shift measured by EELS and XPS for oxides has been suggested to be on the order of the band-gap energy [38], and may arise from many-body relaxation effects (more dominant in XPS) in which nearby electron orbitals are pulled towards a core hole [32]. Table 1 gives an indication of the range of $L_{2,3}$ peak positions expected for each Cr oxidation state and their relative overlap. It is important to note that XPS values are reported as binding energies, not edge maxima. Furthermore, charging of insulating materials in XPS requires the referencing of binding energies to allow comparability of results from different specimens. However, various methods are used for this referencing which lead to binding energy differences of up to 0.5 eV [39]. Therefore, the XPS binding energies in Table 1 should be compared qualitatively.

The EELS measurements of the bacteria examined by EC-TEM and precipitates examined in thin section by conventional TEM are plotted in **Fig. 8b**. The correlation plot (Fig. 8b) indicates that Cr associated with *S. oneidensis* is most consistent with a mean oxidation state of +3 or lower. Measurements of hydrated bacteria in the EC are in good agreement with the analysis of isolated precipitates measured in cross section by conventional TEM. These results illustrate EELS techniques yield accurate data even under the more onerous experimental conditions of the EC.

Collapse of nontronite layers by Fe(III) reduction

We report the first accurate TEM measurements of nontronite layer

The different Cr oxidation states fall within separate regions in the plot and are labeled II, III, and VI. The solid data points represent the mean of the data for a particular Cr standard.
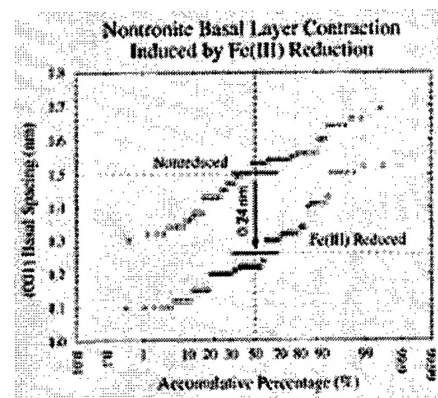

Fig. 10. Distribution of (001) layer spacings in nonreduced and microbially reduced nontronite as measured by EC-TEM. The horizontal bar represents the mean of the distribution.

contraction induced by the reduction of structural Fe(III). A contraction of 0.24 nm in mean (001) layer spacing was observed. Our measurement is consistent with previous *in-situ* X-ray diffraction studies which observed an interlayer contraction of 0.28 ± 0.04 nm in Na-nontronite after $\approx 85\%$ of the Fe(III) was reduced (based on Fig. 8 of [23]). Our TEM measurement was possible because clays were examined in their 'native' hydrated state in an EC. Previous TEM reduction studies used water exchange with methanol and infiltration with L.R. White resin in attempts to preserve the layer spacings of hydrated clay [24]. However, our EC-TEM results suggest the homogeneous layer spacing observed in both reduced and oxidized smectite by Stuki and Tessier [24] results from the interaction between the non-polar methanol and clay interlayer surfaces. In comparison to EC-TEM results, the observation that a homogeneous 1.26 nm (001) layer spacing is produced in the methanol-clay system regardless of Fe(III)/Fe(II) content [24] suggest interlayer forces are effected by the presence or lack of polar water molecules.

We show that established embedding techniques used to study clay reduction do not accurately preserve basal spacings of expandable clays. At least for L. R. White, solvent exchange and resin infiltration contract layer spacings, and therefore cannot be used to study, for example, the correlation between layer spacing and local Fe(III) / Fe(II) composition. In fact, conventional TEM has been unable to even image conclusively the contraction of clay layers induced by Fe(III) reduction. As demonstrated here, conventional TEM specimen preparation artifacts such as clay layer contraction arising from solvent exchange, dehydration, and resin infiltration are avoided by using EC-TEM.

Summary

We demonstrate quantitative EELS oxidation state measurements can be performed using EC-TEM which could provide data lost by conventional specimen preparation. To our knowledge, this is the first demonstration of EELS microanalysis by EC-TEM. We further demonstrate, for the first time using TEM, the collapse of (001) layers of nontronite induced by Fe(III) reduction. This is possible because the clays were examined in their 'native' hydrated state using an EC. The technique of EC-TEM, especially together with EELS, can provide data on mineralogy, spatial distribution, and speciation of metals, necessary for determining the mechanism (s) of microbial metal reduction / oxidation.

Acknowledgements

References

1. Cieslak-Golonka, M., *Polyhedron*, **15**, 3667 (1995).

2. Clesceri, L. S., Greenberg, A. E., and Eaton, A. D. (Eds) *Standard Methods for the Examination of Water and Wastewater*, American Public Health Association, Washington, DC (1999).

3. Hill R. R. H. and Cowley H. M., *S. Afr. J. Sci.*, **82**, 595 (1986).

4. Fude, L., Harris, B., Urrutia, M. M., and Beveridge. T. J., *Appl. Environ. Microbiol.*, **60**, 1525 (I 994).

5. Badar, U., Ahmed, N., Beswick, A. J., Pattanapipitpaisal, P., and Macaskie, L. E., *Biotech. Let.*, **22**, 829 (2000).

6. McLean, J. S., Beveridge, T. J., and Phipps, D., *Environ. Microbiol.*, **2**, 611 (2000).

7. Smith, W. L. and Gadd G. M., *J. Appl. Microbiol.*, **88**, 983 (2000).

8. McLean, J. and Beveridge, T. J., *Appl. Environ. Microbiol.*, **67**, 1076 (2001).

9. Lytle, C. M., Lytie, F. W., Yang, N., Qian. J. H., Hansen, D., Zayed. A., and Terry, N., *Environ. Sci. Technol.*, **32**, 3087 (1998).

10. Paterson, J. H., Krivanek, O. L., *Ultramicroscopy*, **32**, 319, (1990).

11. van Aken, P. A., Liebscher, and B., Styrsa, V. J., Phys. *Chem. Min.*, **25**, 323 (1998).

12. Wang, Z. L., Bentley, J., and Evans, N.D., *J. Phys. Chem. B*, **103**, 751 (1999).

13. Cressey, G., Henderson, C. M. B., and van der Laan, G., *Phys. Chem. Miner.*, **20**, 111 (1993).

14. Daulton T. L., Little B. J., Lowe K., and Jones-Meehan J., *Journal of Microbiological Methods, in press* (2002).

15. Venkateswaran, K., Moser, D. P., Doilhopf, M. E., Lies, D. P., Saffarini, D. A., MacGregor, B. J., Ringelberg, D. B., White, D. C., Nishijima. M., Sano, H., Burghardt, J., Stackebrandt, E., and Nealson, K. H., *Int. J. Syst. Bacteriol.*, **49**, 705 (1999).

16. Stucki, J. W., Komadel, P., and Wilkinson, H. T., *Soil Science Society of America Journal*, **51**, 1 663 (1987).

17. Kostka, J. E., Stucki, J. W., Nealson, K. H., and Wu, J., *Clays & Clay Minerals*, **44**, 522 (1 996).

18. Ravina, I. and Low, P. F., *Clay & Clay Minerals*, **20**, 109 (1972).

19. Kohyama, N., Shimoda, S., and Sudo, T., *Clay &. Clay Minerals*, **21**, 229 (1973).

20. Stucki, J. W., Low, P. F., Roth, C. B., and Golden, D. C., *Clays & Clay Minerals*, **32**, 357 (1984) .

21. Chen, S. Z., Low, P. F., and Roth, C. B., *Soil Sci. Soc. Amer. J.*, **51**, 82 (1987).

22. Shen, S., Stucki, J. W., and Boast, C. W., *Clays & Clay Minerals*, **40**, 381 (1992).

23. Wu, J., Low, P. F., and Roth, C. B., *Clays & Clay Minerals.*, **37**, 211 (1989).

24. Stucki, J. W. and Tessier, D., *Clays & Clay Minerals*, **39**, 137 (1991).

25. Kim, J., Daulton, T., Furukawa, Y., Lavoie, D., and Newell, S., *Geology, submitted* (2002).

26. Myers. C. R. and Nealson, K. H., *Geochim. Cosmochim. Acta,* **52**, 2727 (1988b).

27. Myers, C. R. and Nealson, K. H., *Science*, **240**, 1319 (1988a).

28. Lovley, D. R., Phillips, E. J. P., Gorby, Y. A., and Landa, E. R., *Nature*, **350**, 413 (1991).

29. Llyod, J. R. and Macaskie, L. E., *Appl. Environ. Microbiol.*, **62**, 578 (1996).

30. Keeling, J. L., Raven, and M. D., Gates, W. P, *Clays and Clay Minerals*,

48. 537 (2000).

31. Fukami, A., Fukushima, K., and Kohyama, N., In: Bennett R. H., Bryant W. R. and Hulbert M. H. (Eds.), *Microstructure of Fine-grained Sediments from Mud to Shale,* Springer-Verlag, New York, pp. 321 (1991).

32. Egerton, R. F., *Electron Energy-loss Spectroscopy in the Electron Microscope,* Plenum, New York (1996).

33. Geiger, J., Schmoranzer, H., *J. Mol. Spectrosc.,* **32**, 39 (1969).

34. Leapman. R. D. and Sun, S., *Ultramicroscopy*, **59**, 71 (1995).

35. Pearson, D. H., Ahn, C. C., and Fultz, B, *Phys. Rev. B*, **47**, 8471 (1993).

36. Leapman, R. D. and Grunes, LA., *Phys. Rev. Lett.*, **45**, 397 (1980).

37. Zaanen, J., Sawatzky, G. A., Fink, J., Speier, W., and Fuggle, J. C., *Phys. Rev. B,* 32, 4905 (1985).

38. Leapman. R. D., Grunes, LA., and Fejes, P.L., *Phys. Rev., B*, **26**. 614 (1982).

39. Swift, P., *Surf. Interface Anal.*, **4**, 47(1982).

40. Allen, G.C. and Tucker, P.M., *Inorg. Chim. Acta.,* **16**, 41 (1976).

41. Asami, K. and Hashimoto, K., *Corrosion Science*, **17**, 559 (1977).

42. Moffat, T. P., Latanision, R. M., and Ruf, R. R., *Electrochim. Acta*, **40**, 1723 (1995).

43. Fink, J., Mtiller-Heinzerling, T., Scheerer, B., Speier, W., Hillebrecht, F. U., Fuggle, J. C., Zaanen, J., and Sawatzky, G. A., *Phys. Rev. B*, **32**, 4899 (1985).

44. Neal, A. L., Lowe, K., Daulton, T. L., Jones-Meehan, J., and Little B. J., *Journal of Applied Surface Science. submitted* (2002).

45. Allen, G. C., Curtis, M. T., Hooper, A. J., and Tucker, P. M., J. Chem. Soc., *Dalton Trans.*, **16**, 1675 (1973).

46. Krivanek, O. L. and Paterson, J. H., *Ultramicroscopy.* **32**, 313 (1990).

47. Ikemoto, I., Ishii, K., Kinoshita, S., Kuroda, H., Alario-Franco, M. A., and Thomas, J. M., *J. Solid State Chem.*, **17**, 425 (1976).

48. Kendelewicz, T., Liu, P., Doyle, C. S., Brown, G. E., Nelson, E. J., and Chambers, S. A., *Surf. Sci.*, **424**, 219 (1999).

49. Konno, H., Tachikawa, H., Furusaki, A., and Furuichi, R., *Anal. Sci.,* **8**, 641 (1992).

50. Brydson. R., Garvie, L. A. J., Craven, A. J., Sauer, H., Hofer, F., and Cressey, G., *J. Phys.: Condens. Matter*, **5**, 9379 (1993).